Incorporating Crosslinks in Fused Filament Fabrication: Molecular Insight

into Post Deposition Reactions

S. Connor Perryman¹, Mark D. Dadmun^{1,2}

¹Department of Chemistry, University of Tennessee, Knoxville, Tn 37996, USA

²Chemical Sciences Division, Oak Ridge National Laboratory, Oak Ridge, TN 37831, USA

Corresponding authors: dad@utk.edu

Abstract: 3D printed objects suffer from intrinsic mechanical weakness due to low interlayer adhesion and defects

that result in anisotropy in their mechanical properties. In this report, we examine the ability of a protocol to

incorporate covalent bonds between layers to strengthen interlayer adhesion by depositing multi-amines between

layers during the fused filament fabrication printing process. The multi-amines may then react with oxygenated

functional groups on the deposited filament to form covalent crosslinks between layers. Determination of the

interfacial fracture energy and infrared (IR) spectroscopy studies indicate the successful formation of covalent bonds

and strengthening of the interlayer interface with a variety of multi-amines. More importantly, IR results also elucidate

the relative rate of reaction of the amines with oxygenated functional groups found on the oxidized filament. These

results show that the crosslinking reactions primarily occur shortly after deposition of the filament, i.e. at elevated

temperatures. The data also show that the reactivity of the amines is not the prevailing factor in determining interfacial

strength, as the aromaticity of the crosslinker plays a key role in creating a stronger interface. These results therefore

provide important foundational understanding that can be used to apply this protocol to a variety of extrusion based

additive processes and materials.

1

1. Introduction

Fused filament fabrication, or FFF, is an additive manufacturing method used in rapid object design and prototyping for thermoplastic materials. Since its conception in the 1980's, the format has expanded to numerous areas including the construction and automotive industries. The ability to generate larger complex objects with minimal waste has driven interest in developing FFF into a reliable and robust manufacturing method. Large-scale printers have been produced and continue to evolve with the goal of advancing the technology to compete with traditional industrial fabrication methods.^{1, 2} Structural weakness and anisotropy that emerge from weak layer interfaces and structural defects remain limiting factors in the advancement of polymeric extrusion based additive technologies beyond the maker level. For instance, a car body produced by the Big Area Additive Manufacturing 3D printer exhibited poor interfacial adhesion during the print process. Talagani et al. developed an efficient method to determine problem areas in the print build where interlayer delamination is probable.³

The FFF print process begins with a CAD model of the desired structure, which is interpreted by the printer's onboard software to move a hot nozzle in the x and y directions above a heated bed surface. Polymer filament is then extruded onto the heated bed to generate each layer with the nozzle moving upwards after layer completion at a predetermined height value in the z-dimension and directed to deposit the next layer. This process is repeated continuously for each layer until the object is fabricated. Inferior mechanical integrity of prints is linked to this layered build process, with mechanical strength dependent on direction of the applied force relative to build orientation (Fig. 1a). This weakening causes structural anisotropy, which is associated with minimal diffusion of thermoplastic between individual layers. Moreover, the bottom portion of prints are subjected to continuous heating from the heated bed with a thermal gradient emerging as the print increases in height along the z-axis. This gradient of thermal energy causes deposited material near the middle and end of prints to cool more rapidly from convection and prevents polymer chains from diffusing across the interlayer boundary to enhance isotropy. Therefore, each layer receives a varying amount of heat from the hot nozzle head as it is built. Cumulatively observed, the print object is subject to a complex thermal history that fluctuates at each layer with respect to the nozzle head, distance from the bed, and the temperature of the print environment (Fig. 1b).

Previous experiments have focused on modifying physical print parameters to reduce anisotropic weaknesses. Raster mechanics and the resulting tensile property changes with raster width, angle, pattern, and spacing

have been analyzed extensively.^{11, 12} Other factors, such as layer height and the extrusion, bed, or air temperature have also been found to influence tensile anisotropy.⁴ Any decrease in anisotropy attained in these studies is due to variation in the amount of interfilament diffusion and the size of void spaces between filaments during the build process, but these factors fail to significantly limit anisotropy. Recent research has therefore shifted from altering these physical print parameters in favor of modifying the polymeric filament itself. Alterations of the printed thermoplastic include the inclusion of additives, such as graphene, microdiamond aggregates, or other reactive components to the filament.^{7,}

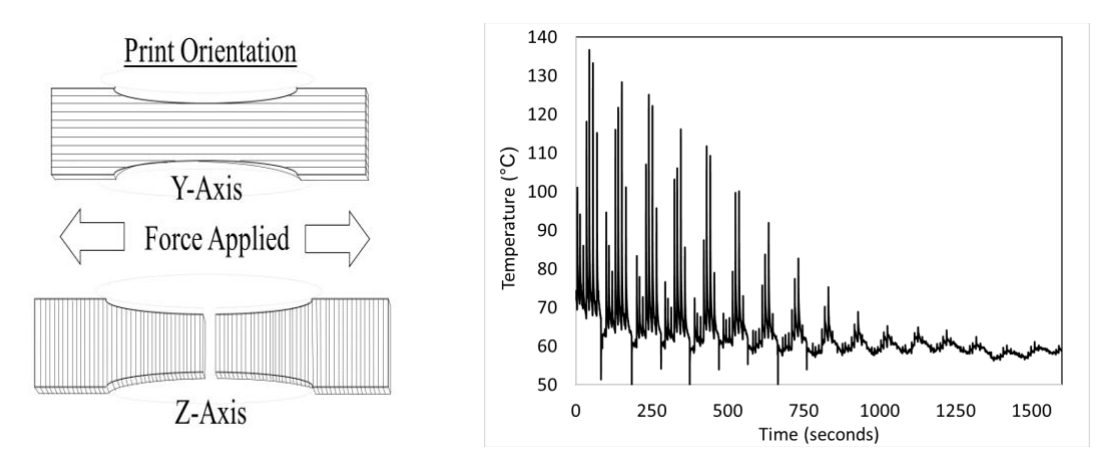


Fig. 1. a. Illustration of an FFF object's build orientation and physical response to an increasing uniaxial force **b.** Thermal history of an individual layer in a sample cube as recorded via thermal camera

ABS, or Acrylonitrile-Butadiene-Styrene, is a terpolymer and common material used in FFF for prototyping. The composition of the ABS can vary significantly among providers; however, two-thirds of the material usually consists of a styrene-co-acrylonitrile (SAN) copolymer matrix interspersed with polybutadiene (PB) domains. It is well established that, when heated at or above 100°C in air, ABS oxidizes to form functional groups such as carbonyls, hydroxyls, and epoxides through reaction of butadiene double bonds with atmospheric oxygen. ¹⁶⁻¹⁸ In the process of filament creation and extrusion, ABS is consistently subjected to temperatures well above 100°C, providing pathways to produce these oxidative groups at the surface of a printed object. These functional groups can then react with properly designed co-reactive molecules in deposition processes that are consistent with 3D printing. Moreover, the reaction of multi-functional molecules between filaments may form *interlayer* covalent bonds, providing a significant increase in interlayer adhesion of the printed object.

Amines are interesting candidates as such crosslinkers, as they readily react with ketones or aldehydes to produce imines. Amines also react with epoxy resin oligomers to produce extensive crosslinks. Thus, in the current study, the formation of interlayer covalent bonds between oxygen containing functional groups on ABS filament that are formed during printing and multi-amines is examined as a rational method to strengthen inter-layer interfaces formed during FFF. The impact of amine structure, loading, and surface temperature on the success of the inter-filament crosslinking reaction are studied from both a mechanical and reactive rate perspective. These results presented below therefore provide insight that can be used to formulate and optimize crosslinking reactions between filaments and open new routes to fabricate more robust and isotropic materials by extrusion-based 3D printing in a scalable fashion.

2. Experimental

2.1 Materials

2.85 mm diameter ABS filament was purchased from Gizmo Dorks. Unmodified polybutadiene (5K M_w), 4,4'-diaminodiphenyl methane (DADPM), 4,4'-diaminodicyclohexylmethane (DADCM), and pentaethylene hexamine (PEH) were purchased from Sigma-Aldrich and used without further purification. KBr windows were purchased from Pike Technologies. Solutions applied to the 3D printed structures during the printing process were generated by dissolving weight percentages of 5, 10, and 20% crosslinker into 10mL of acetone at room temperature. The molecular structure of each crosslinker is shown in Figure 2.

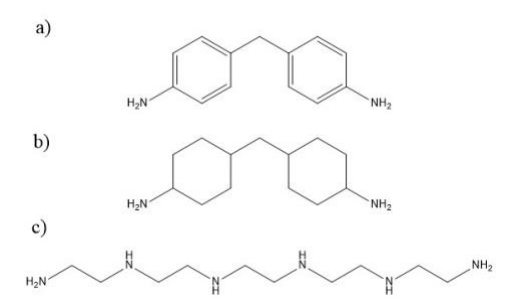


Fig. 2. Chemical Structures of the crosslinkers used in this study **a.** 4,4-diaminodipheny methane, **b.** 4,4'-diaminodicylohexylmethane, and **c.** pentaethylene hexamine

2.2 Interfacial Adhesion Determination

Interfacial adhesion experiments in this study monitored specific factors that influence the interlayer strength of the samples. Samples prepared using crosslinker solutions with concentrations from 0 to 20 wt% were first

examined to illustrate how the interface is strengthened by increasing reactive crosslinker concentration. A second set of samples were examined to elucidate the impact of decreasing available thermal energy for the crosslinking reactions by increasing stop times between layer deposition. Samples tested under these criteria consisted of both unmodified and 5 wt% crosslinker. Lastly, to demonstrate the crosslinker's overall effectiveness on an entire printed structure, the tensile properties of a samples printed with crosslinker deposited on every layer were monitored. In these studies, the tensile properties of the printed structure was determined both parallel and perpendicular to the print direction to document the impact of the incorporation of crosslinks on structural anisotropy of the printed parts.

Specimens were created from hollow cubes printed with a Lulzbot Taz 5 printer and ABS filament with diameter of approx. 2.85mm and a nozzle head of 0.5mm. Cubes consisted of 176 layers printed at 60mm/s with a 0.3mm layer height for a total object height of approximately 53mm (Fig. 3a). Print parameters for each cube included 210°C extrusion temperature and a bed temperature of 110°C to maintain similar thermal and build history for all samples. Crosslinker solutions were applied to the middle sixteen layers of each cube in a single counter-clockwise motion by soaking cotton swabs in the solution and 'painting' the solution onto the filament. By utilizing this swabbing technique, a thin film of crosslinker solution is delivered to inter-filament interface. Reproducibility of interfacial adhesion values are consistent indicating a reasonably regular dosage of the crosslinker on each layer. Completed cubes were then cut at each face corner with a Dremel® rotary saw to yield individual plaques. The cube faces were then cut with a laser cutting system to create tensile samples for Instron testing (Fig. 3b). Shape and dimensions of the dual-cantilever beam samples were derived from previous literature used to test the interlayer strength of FFF objects by isolating the tensile force of separation into a preset "crack" of approximately 3 layers wide that would separate specifically at the modified interface.^{2, 20} To establish a statistically relevant adhesion strength for each crosslinker, a minimum of two cubes per solution were generated, which creates eight tensile samples. Specimens that examined the influence of print pause time on interlayer adhesion were created by first pausing the print at a layer, applying solution with the same method as other prints, waiting for a set amount of time, and then allowing the print to continue with the next layer. This process was applied to the central three layers in the middle sixteen that received crosslinker solution to allow the pause time to only affect the test interface.

The interfacial strength of each sample was determined with an Instron Model 5567 universal tensile testing device set with a 30kN load cell. Samples were pulled apart at a rate of 2.1E-3 mm/s until failure at the test interface.

Testing rates were kept at a low speed to accurately measure the fracture energy at the crosslinker modified interface and to prevent the unmodified layers of the samples from separating due to rapid onset mechanical forces. Results generated by this experiment include sample displacement at break, the Young's modulus, and maximum tensile strength. This data were then used to calculate the interfacial fracture energy, as discussed in the results section of this study. Specimens that examined the influence of print pause time and the subsequent decrease in layer temperature on interlayer adhesion were created by first pausing the print at a layer, applying solution with the same method as other prints, waiting for a set amount of time, and then allowing the print to continue with the next layer. This process was applied to the central three layers in the middle sixteen that received crosslinker solution to allow the pause time to only affect the test interface. Pause times consisted of 0, 10, and 20 minutes between individual layer deposition. In the final tensile study, a single cube was printed with an application of 10wt% DADPM solution to every layer and subsequently laser cut into ASTM D638-V standard tensile dogbones with a set oriented parallel to the layer build and another transverse to the layer build. Tensile properties were then determined for the crosslinked and ABS prints at 1mm/min.

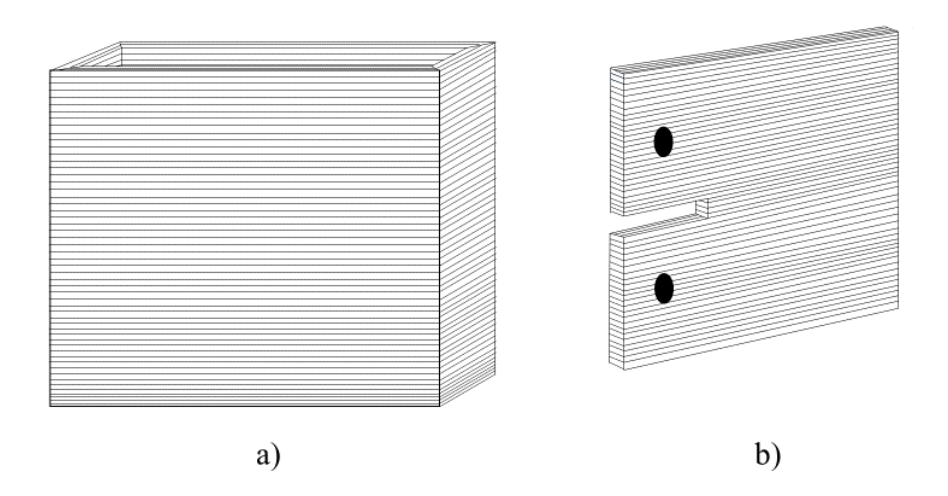


Fig. 3. a. Illustration of printed sample cube and **b.** Double Cantilever beam sample machined from cube 2.3 Infrared Spectroscopy of butadiene oxidation.

Polybutadiene was oxidized at 200°C in open air for ten minutes in 2.5g batches in a glass petri dish via hot plate. Solutions of oxidized polybutadiene with 10 and 30 weight percent crosslinker were formed in dichloromethane. These mixtures were then drop cast via syringe onto KBr windows, air dried at room temperature for 30 minutes, and annealed in a vacuum oven at 90 or 110°C to mimic the thermal environment of a printed layer. Samples were then

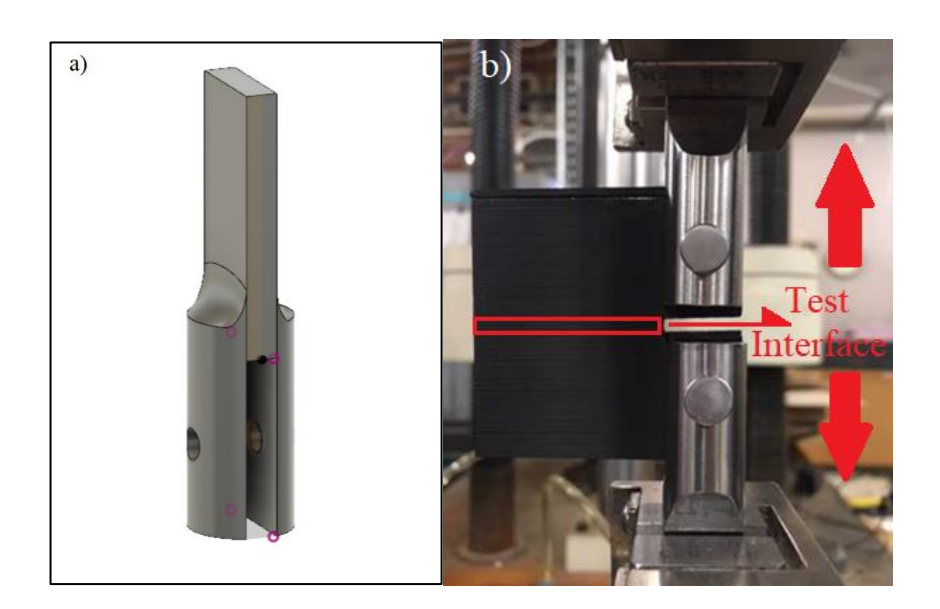
periodically removed at set time periods and IR spectra were obtained with a Thermo Scientific Nicolet iS50 FT-IR device at 64 scans with 0.4 cm⁻¹ resolution.

3. Results and Discussion

3.1 Mechanical Testing and Quantifying Crosslink-Induced Isotropy

The impact of crosslinker addition on interlayer adhesion was determined by measuring the fracture energy of the inter-filament layers using a dual cantilever beam protocol as reported in the literature.^{1, 20} Cube samples were printed and cut to fit a custom test geometry (Fig. 4). These samples were then pulled apart on an Instron machine with the stress and strain monitored. The interfacial fracture energy, G, is then determined from Equation 1, where P is the load at tensile failure, δ is the sample displacement at break, b is the sample thickness (4.5mm), and A_0 is the initial crack length (15mm).¹ (Fig. 4c).

$$G (fracture \, energy) = \frac{3P\delta}{2bA_0}$$
 Equation 1



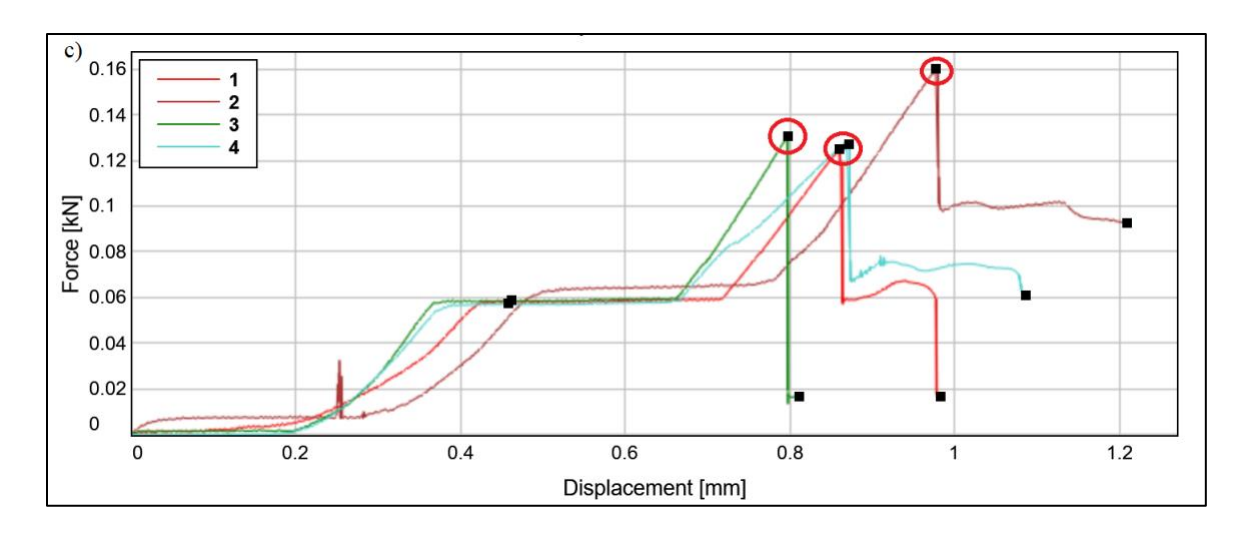


Fig. 4. a. 3D model of Instron grips for tensile tests **b.** Image of tensile sample tested with Instron and **c.** Typical force vs. displacement curve of fracture energy tests

Initial fracture energy measurements were completed with neat ABS samples to establish the baseline interfilament adhesion present in the printed structure. Neat ABS samples failed along the interface with an average fracture energy of ~1.1 kJ/m². This value is consistent with results observed for neat ABS tested at similar conditions.¹ Crosslinker solutions of varying weight percent were then applied to the interfilament interface to document the ability of any crosslinking reaction to strengthen the inter-layer interface. The strength of the interface was monitored for the addition of 5, 10 and 20 weight percent solutions of crosslinker. The average fracture energy of printed specimens increases with the addition of the crosslinker, and increases with the crosslinker concentration, as shown in Fig. 4a.

The results in Fig. 5a show that DADPM strengthens the interface most effectively, with marginal improvement from PEH until higher concentrations while DADCM strengthens the interface at lower loadings, but is less effective at 20%. This is further evidenced by Fig. 6 where the DADPM crosslinking improves the tensile properties of the sample in both the longitudinal and transverse orientations, increasing the Young's modulus by approximately 7 and 5% respectively. Given that the PEH has five amines available for reaction with oxygenated functionalities, while DADCM and DADPM have two, it is clear that the number of reactive functionalities in the crosslinker molecule is not the most dominant factor impacting the success of crosslinking reactions. The fact that PEH is a less effective crosslinker is surprising as amine chemistry would suggest that PEH may react most readily with oxygenated functional groups due to its sterically unhindered structure, abundance of primary and secondary amines, and higher general nucleophilicity/basicity.^{21, 22} The nucleophilicity of the PEH amines is also enhanced by

the alkylic structure of the molecule, as opposed to the aryl nature of DADPM that limits it's nucleophilicity by the electron-distributing mesomeric effect.

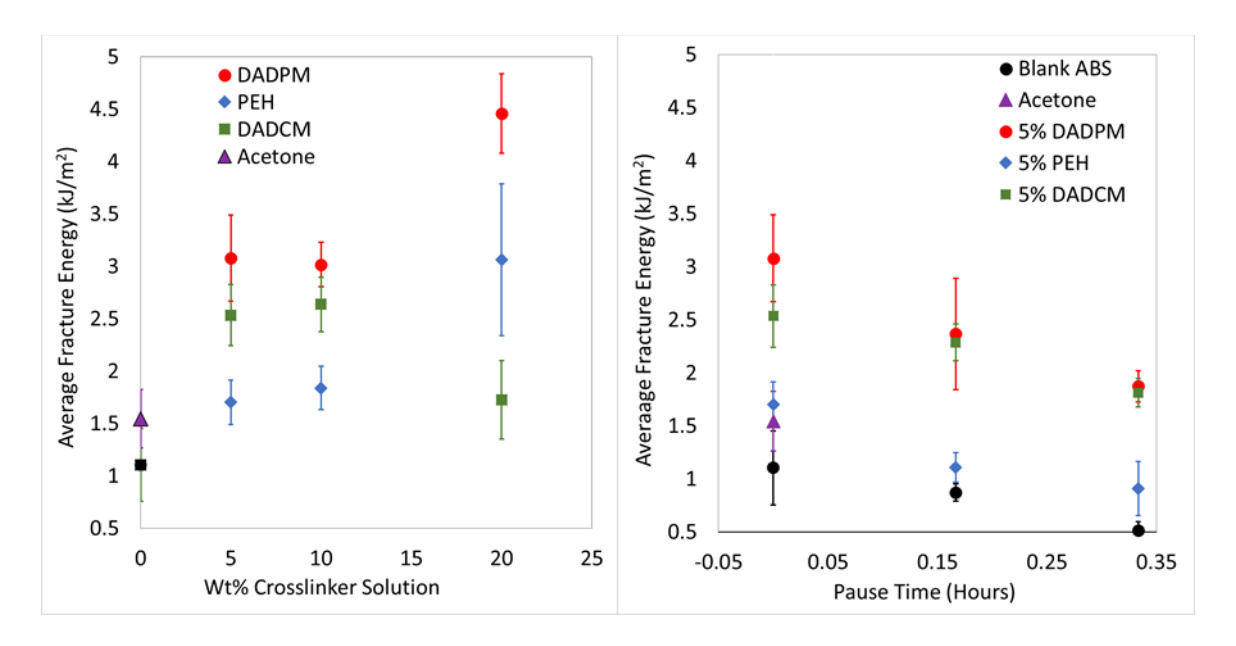


Fig. 5. a. Average tensile fracture energy as a function of crosslinker concentration **b.** Interfacial fracture energy as a function of print pause time

3.2 Adhesion Measurements with Varying Print Pause Time

As fused filament fabrication scales up to create larger structures such as cars and houses, the time to build a layer increases. A direct result of this scaling up is that the supporting layer may cool significantly by the time the next layer is deposited, weakening the interface. In order to examine the ability of this protocol to enhance interfacial adhesion on cooled beads, samples were fabricated with deliberate pause times between layers. The impact of incorporating crosslinkers between the paused layers on the interlayer adhesion was then monitored by similar interfacial adhesion measurements. Fig. 5b. demonstrates the change in fracture energy of the modified interlayer interfaces with print pause time. Longer pause times allow the sample to cool more, permitting filament to drop below the glass transition temperature, reducing interfilament diffusion and weakening the interface. As the pause time increases, the thermal energy available for the crosslinking reactions also decreases, potentially resulting in a decrease in interfacial adhesion in the crosslinked samples as well.

It is interesting to note that the interfacial adhesion of the PEH modified interfaces decreases to values similar to unmodified samples with pause time. This result illustrates, again, that interfacial strengthening reactions are not strongly coupled to crosslinker reactivity. In fact, the DADCM and DADPM modified interfaces maintain fracture energies that surpass the strength of the un-paused, unmodified ABS interface for all pause times.

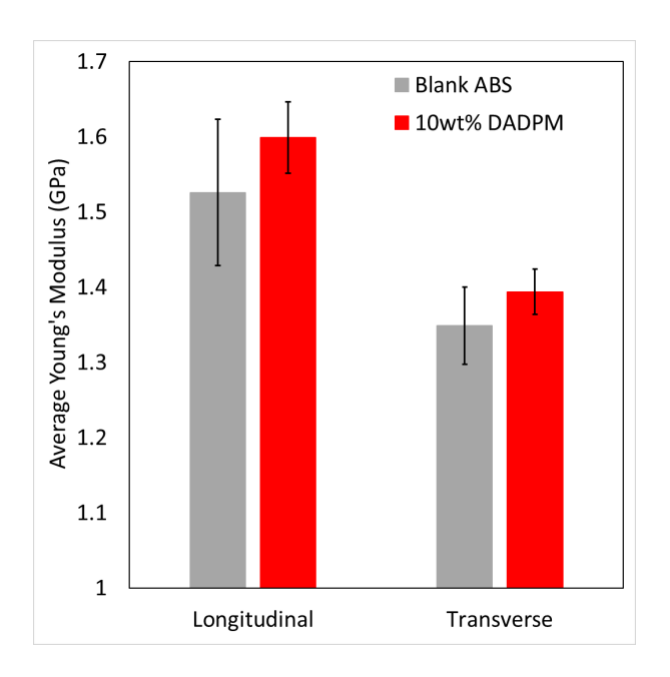


Fig. 6. Modulus of printed tensile dogbones with and without crosslinker applied to each layer

3.3 Reaction Kinetics via Infrared Spectroscopy

The interfacial adhesion results are consistent with the formation of interlayer crosslinks from the reaction of the multi-amine and the oxidized filament. To provide more insight into the impact of crosslinker structure on the kinetics of these reactions, infrared spectroscopy was used to follow the reaction of oxidized polybutadiene (Ox-PB) and the amine crosslinkers to model the reactions that occur in the printing process. Polybutadiene is one of the three components present in ABS and the primary component that undergoes oxidation necessary to form functionalities that will react with amines to form interlayer crosslinks. Thus, we expect that the FTIR based reaction results presented will closely follow the reactions that occur in the printed part. The amines may react with a range of oxygenated functionalities. For instance, it is known amines react with hydroxyl groups, where the reactivity increases in proportion to the number and type of hydroxyl functionalities.²³ In more detail, hydroxyl groups that neighbor epoxides may reposition the methylene carbon for more entropically favorable nucleophilic attack from amines, providing one example of how the oxidation of the butadiene in the ABS filament facilitates the formation of interlayer

crosslinks by reaction with amines to strengthen interlayer interfaces as the object is built. By monitoring the direct reactions of the additives with oxidized polybutadiene under thermal conditions that mimic printed filament temperatures, a qualitative understanding of the impact of amine structure and reactivity on the formation of interfilament crosslinks is obtained that can then guide the choice of crosslinker structure.

In these experiments, solutions of oxidized polybutadiene and each crosslinker at 10 or 30 weight percent in dichloromethane were dropped onto KBr discs. These films were then annealed at 90 or 110°C for extended periods of time. The choice of annealing temperature was guided by measurements from an infrared camera (FLIR A35sc) that recorded the temperature of a single layer on a sample cube printed under the same conditions as the crosslinked samples. The IR thermal camera was placed within 1-2 ft of the printed sample cube. The temperature of the crosslinked layers were then recorded by the camera (Fig. 7a) as a function of time with the same conditions as those observed in Figure 1b. Temperature measurements begin when a layer is deposited and end when the print was completed. The reported temperature of the crosslinked layers is the time average of the instantaneous tempratures that include temperature elevations due to proximity of the hot extruder during deposition of subsequent layers as shown in Figure 1b. The temperature is averaged over *ca.* 100 second intervals that correspond to the printing of a single layer. These average filament temperatures are then plotted as a function of the print time. These results are shown in Figure 7b, which show that the deposited filament starts slightly above 110 °C and then drops to 90 °C in approximately four minutes. Thus, these temperatures mimic the thremal history and monitor the potentail reaction during the first few minutes after bead deposition.

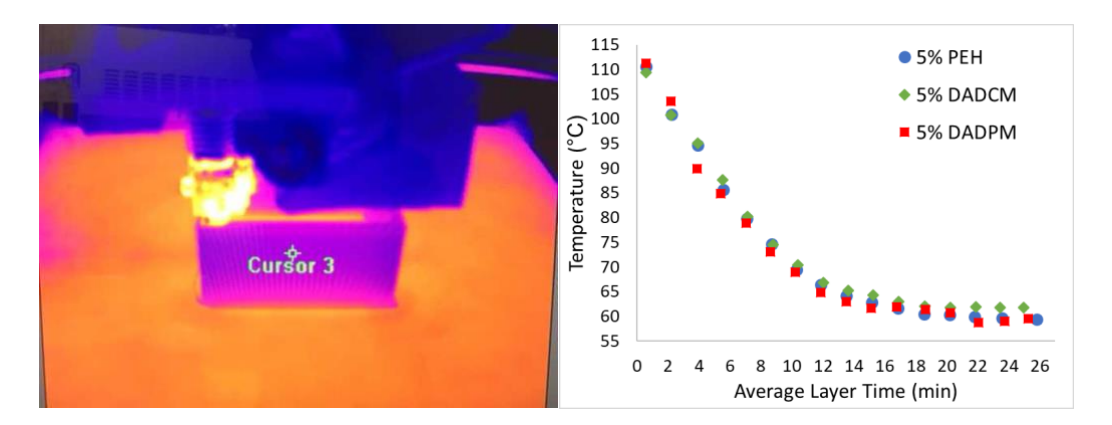


Fig. 7. a. Thermal imaging of a cube print, with identification of temperature measurement site (green crosshairs) and **b.** Averaged temperature of the designated layer as a function of the time after layer deposition.

Peak assignments associated with crosslinker amine motion were obtained from IR spectra analysis of the pure materials. An in depth description of DADPM's spectrum and subsequent peak assignments has been reported in the literature.²⁴ Two peak pairs in the 3300-3415cm⁻¹ region were designated for the assymetric and symmetric stretching of the primary amine's hydrogens (Fig. 8b). During sample annealing, the reaction progress of the primary amine was monitored from the relative decrease of the intensities of these peaks. Using DADPM peak assignments as a reference, the pure spectrum of DADCM and PEH were also analyzed and curve fitted for their individual amine moieties. Full peak assignments for each species are listed in Table 1. Drop-cast IR samples were then annealed at increasing annealing times and monitored for changes in peaks or the creation of new peaks associated with newly formed bonds by reaction of the crosslinker. In the DADPM mixtures, the formation of a secondary amine stretching peak (≈3380cm⁻¹) was observed beyond two minutes of annealing at 110°C as seen in Fig. 8a. DADCM mixtures generated a similar peak at approximately 3330cm⁻¹ signifying secondary amine creation. The growth of these secondary amine peaks are interpreted to indicate the formation of a crosslink between the amine and the oxidized polybutadiene matrix with annealing time. Further analysis of the time evolution of these peaks is then used to qualitatively monitor the reaction kinetics of the individual crosslinker molecules with oxidized polybutadiene in hopes of providing more insight into the driving forces that guide the interlayer strengthening observed above.

Table 1Infrared signal assignments for Oxidized Polybutadiene and Crosslinker

Species	Wavenumber (cm ⁻¹)	Assignment
Polybutadiene	3510	Free O-H Stretch
	3430	O-H Stretch H-Bonded to Carbonyl
	3270	O-H Stretch H-Bonded to Hydroxyl
4,4-Methylenedianiline	3444/3414	Asymmetric NH ₂ Stretch
	3380	Secondary Amine Stretch
	3336/3317	Symmetric NH ₂ Stretch
	3208	Aromatic C-H Stretch
Pentaethylene Hexamine	3359	Primary Amine Stretch
	3293	Secondary Amine Stretch
4,4'-Diaminodicyclohexylmethane	3348	Asymmetric NH ₂ Stretch
	3290	Symmetric NH ₂ Stretch

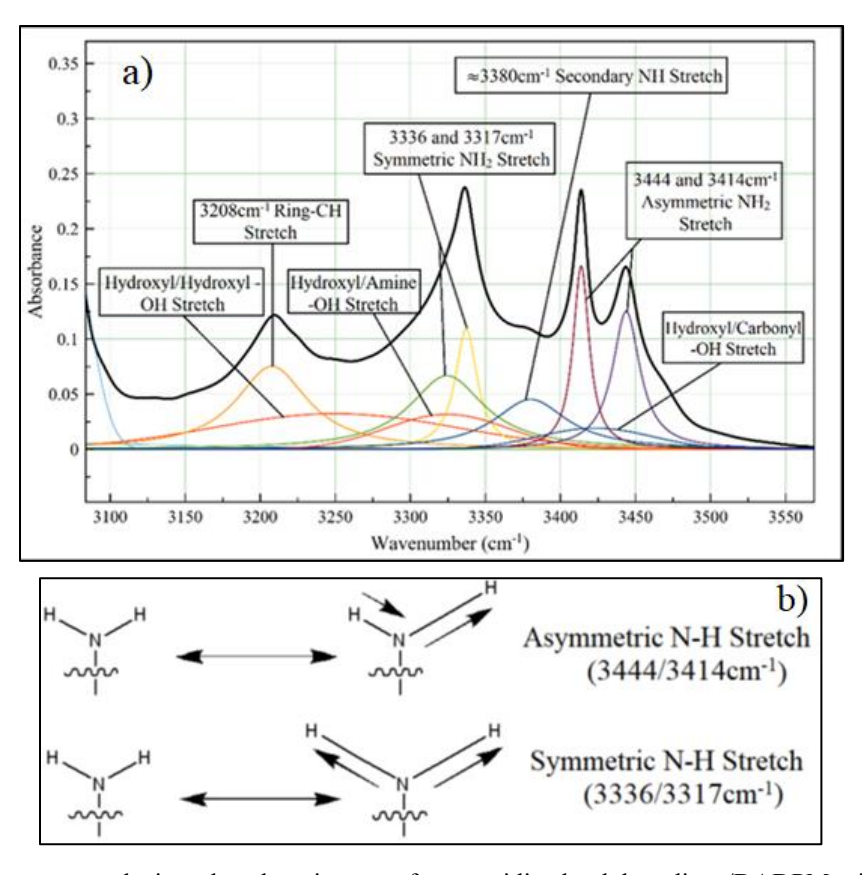


Fig. 8. a. Infrared spectra analysis and peak assignment for an oxidized polybutadiene/DADPM mixture and **b.** Atomic stretching and signal assignment of DADPM's primary amine

3.4 Qualitative Analysis of Reaction Kinetics

Possible reactions that will result in crosslink formation between filaments include the reaction of a primary amine with an oxygenated functional group and the subsequent reaction of a secondary amine to a different oxygenated functional group. Thus, the kinetics of the crosslinking reactions are modeled using equations that account for both these reactions.

Primary Amine Depletion =
$$k_1[PBOx]^x[-NH_2]^y \approx k_1'[-NH_2]^y$$

Secondary Amine Depletion = $k_2[PBOx]^x[-NH]^z \approx k_2'[-NH]^z$
 $k_1' + k_2' = k'$ (Combined Pseudo Rate Constant)
 $[PBOx]^x$ (Oxidized Polybutadiene)

Though the exact amount of oxidative functional groups present in the polybutadiene is unknown, it is assumed to be relatively constant for a given oxidation process, and is thus combined with the reaction rate constant k_1 (k_2) to create a pseudo rate constant k_1 (k_2). The area under the curve of the relevant peaks were then plotted as a function of annealing time. To monitor the reaction of primary amines, the asymmetric amine stretching modes designated by 3414 cm⁻¹ (DADPM), 3348 cm⁻¹ (DADCM), and 3359 cm⁻¹ (PEH) were monitored. In the analysis of the infrared spectra, the pair of asymmetric amine signals were found to be consistently distinct from one another, allowing for a more reliable peak fit to monitor the reaction. Similar designations of secondary amine stretches; 3375 cm⁻¹ (DADPM), 3330 cm⁻¹ (DADCM), and 3293 cm⁻¹ (PEH) were used to follow the reaction of secondary amines. Peak normalization was conducted by dividing the individual peak areas at given reaction times by the initial peak area prior to the heating.

Figure 9 shows the change in the amount of primary (9a) and secondary (9b) amines in the oxidized polybutadiene and 10% DADPM films with reaction time that are annealed at 90°C and 110°C. Figure 7a shows that the loss of primary amine in the reaction of DADPM and oxidized polybutadiene reaches steady state after approximately 5-10 minutes when annealed at 110°C. However, annealing at 90°C does not attain a steady state primary amine concentration even after 40 minutes. Inspection of Figure 9b shows that the concentration of secondary amines grows at early times, which is coincident with the loss of primary amine. The amount of secondary amine decreases as well at longer times, signifying the further reaction of the secondary amines with the oxidized polybutadiene until the primary amines are fully converted at around 40 minutes. The pseudo rate constant, k_1 ', for this primary amine reaction is then determined by taking an average slope of the data below 10 minutes (i.e. before steady state) for the data at 110°C and for the whole annealing time for the data at 90°C. Similarly, the loss of secondary amine from 10 to 40 minutes for the sample annealed at 110°C provides the pseudo rate constant k₂'. k₁' and k_2 ' can then be added to offer a qualitative total rate constant of the reaction ($k' = k_1' + k_2'$) between a given amine with oxidized polybutadiene. Figure 10 shows the same change in amine concentration with annealing time for the oxidized polybutadiene and 30% DADPM films, while Figure 11 shows the time evolution of the amine concentrations for the reaction of DADCM with oxidized polybutadiene and Figure 12 provides the same evolution of the reaction of PEH with oxidized polybutadiene. The pseudo rate constants k_1 , k_2 , and k for these reactions are also derived from these plots as described above.

It is important to emphasize that these rate constants are only meant to provide insight into the relative reactivity of DADPM, DADCM, and PEH with oxidized polybutadiene. This analysis monitors the relative reactiveness of each crosslinker solely during the high temperature portions of a layer's thermal history (90-110°C). Thus, the clearly qualitative nature of the analysis provides insight into the underlying factors that control the relative rate of formation of crosslinks in the proposed 3D printing protocol only for these potential crosslinkers.

Figure 13 shows the change in k₁' and k₂' (11a) as well as k' (11b) for DADPM at 10% and 30% loading and both annealing temperatures. This data quantifies the extent to which the reaction of the primary amine is (significantly) faster than the secondary amine reaction rate, verifying that the reaction of the primary amine dominates the success of the crosslinking reactions. This data also quantifies how much faster the reaction of DADPM with oxidized polybutadiene is at 110°C than at 90 °C and how changing the DADPM concentration impacts the reaction rate. Clearly most of the reaction between DADPM and oxidized polybutadiene occurs at elevated temperature, is between the primary amine and oxygenated functionalities, and is more efficient with higher amine loading.

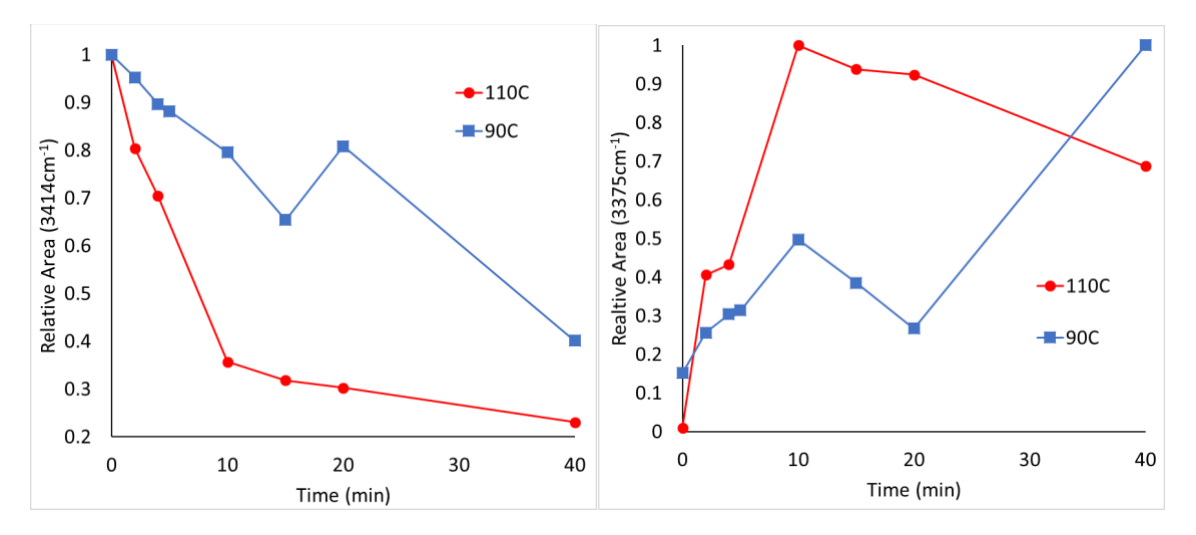


Fig. 9. a. Relative peak area of primary amines and **b.** Secondary amines as a function of annealing time for 10 wt% DADPM and oxidized PB

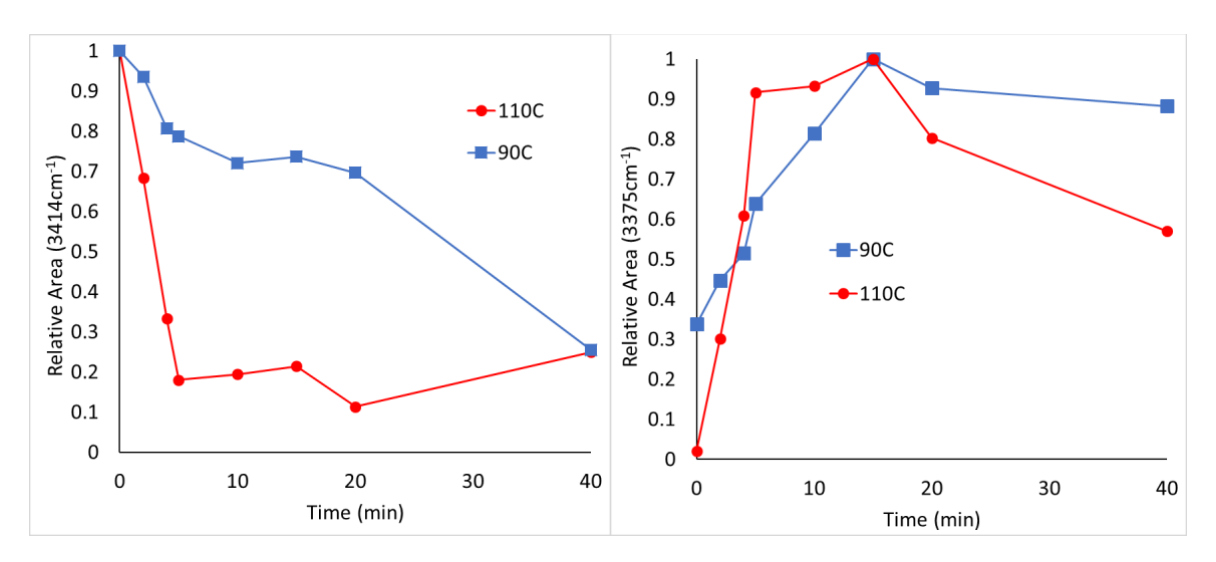


Fig. 10. a. Relative peak area of primary amines and **b.** Secondary amines as a function of annealing time for 30 wt% DADPM and oxidized PB

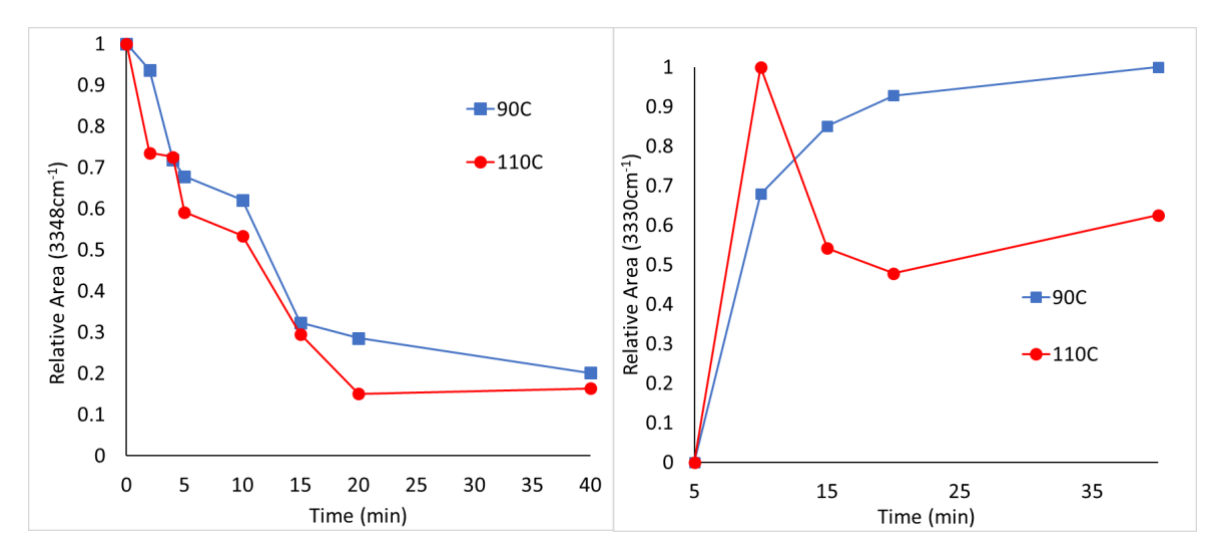


Fig. 11. a. Relative peak area of primary amines and **b.** Secondary amines as a function of annealing time for 10 wt% DADCM and oxidized PB

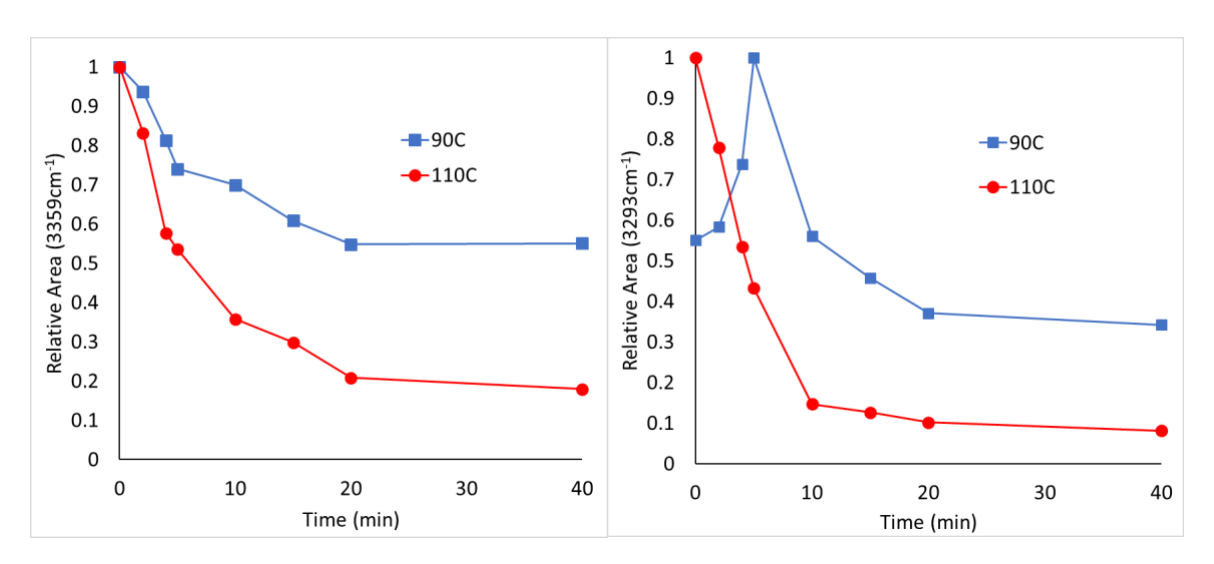


Fig. 12. a. Relative peak area of primary amines and **b.** Secondary amines as a function of annealing time for 10 wt% PEH and oxidized PB

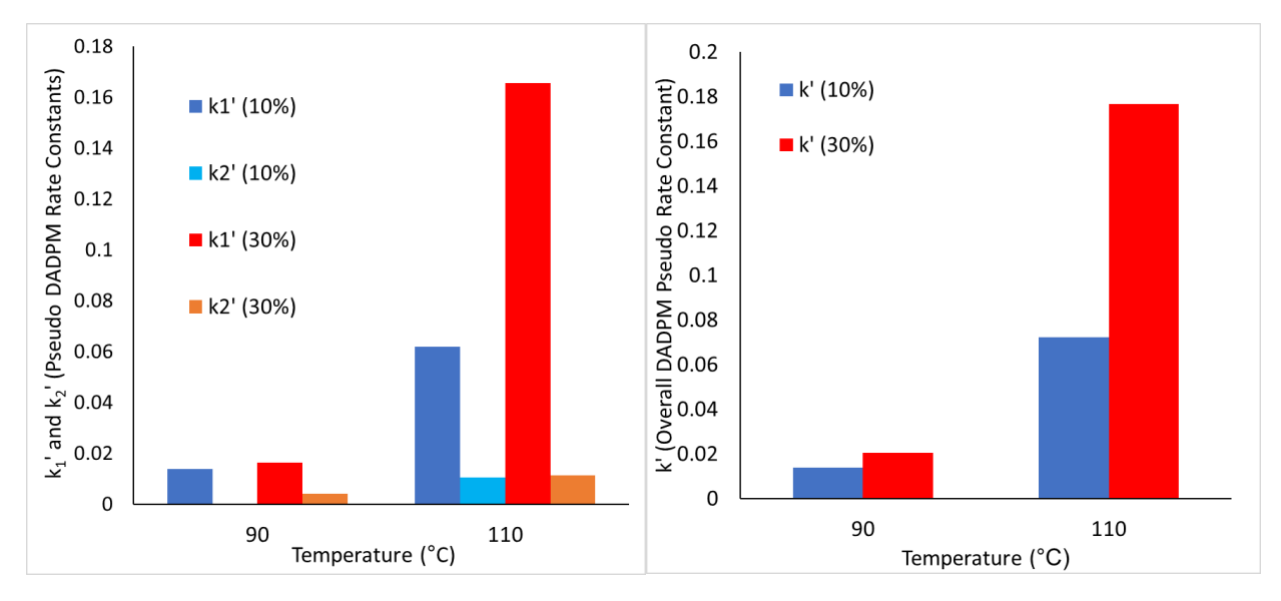


Fig. 13. a. Primary (k₁') and secondary (k₂') DADPM amine rate constants and **b.** Combined (k') DADPM reaction rate constants at different annealing temperatures

Similar behavior is found for the reaction of DADCM and PEH with oxidized polybutadiene, except that the rate of reaction of DADCM with Ox-PB is less dependent on temperature. Figure 14 shows the pseudo rate constants of the primary amine reactions with Ox-PB (Fig. 14a), the reactions of the secondary amines with Ox-PB (Fig. 14b) and the overall reaction rate constants (Fig. 14c) for 10% amine loading. Inspection of these values leads to the interpretation that the reaction of the DADPM primary amine at 110°C is significantly faster than other reactions, but that the reactions of DADCM is less dependent on temperature than that of PEH or DADPM. The reaction of the secondary amines of PEH with Ox-PB are more prevalent than in DADCM or DADPM, presumably because the PEH

contains secondary amines in its structure, and thus is more available for reaction. These results are in general agreement with the general reactivity of aliphatic, cycloaliphatic, and aromatic amines as curing agents in epoxy thermosets. It is well known that primary amines react more rapidly with epoxy functionalities than secondary amines which matches well with the results of Figure 14.^{25, 26} The primary amine reaction rate constant (k_1) of both DADPM and DADCM are consistently higher than the secondary reaction rate constant (k_2) .

Correlation of these results to the interfacial fracture energy (Figure 5) leads to some interesting insights. Reaction of DADPM with the oxidized polybutadiene in the printed structure yield the strongest inter-layer adhesion, with DADCM exhibiting the next strongest at low amine loadings, and PEH providing significant interlayer strength at the highest loading. Combining knowledge of the interlayer thermal history during printing (Figure 7b) and the relative amine reactivity with Ox-PB, we come to the conclusion that the amine-Ox-PB reactions occur in the first few minutes of the print process at elevated temperature. This is the condition where the DADPM reaction dominates over that of the other two amines. If the reaction between amine and Ox-PB occurred at lower temperature or the reaction of the secondary amines also significantly contributed to the interfacial strengthening, DADCM or PEH would show stronger interfaces. The fact that PEH shows significant strengthening of the interface at high loading suggests that the reaction of the secondary amine can become important at higher loadings.

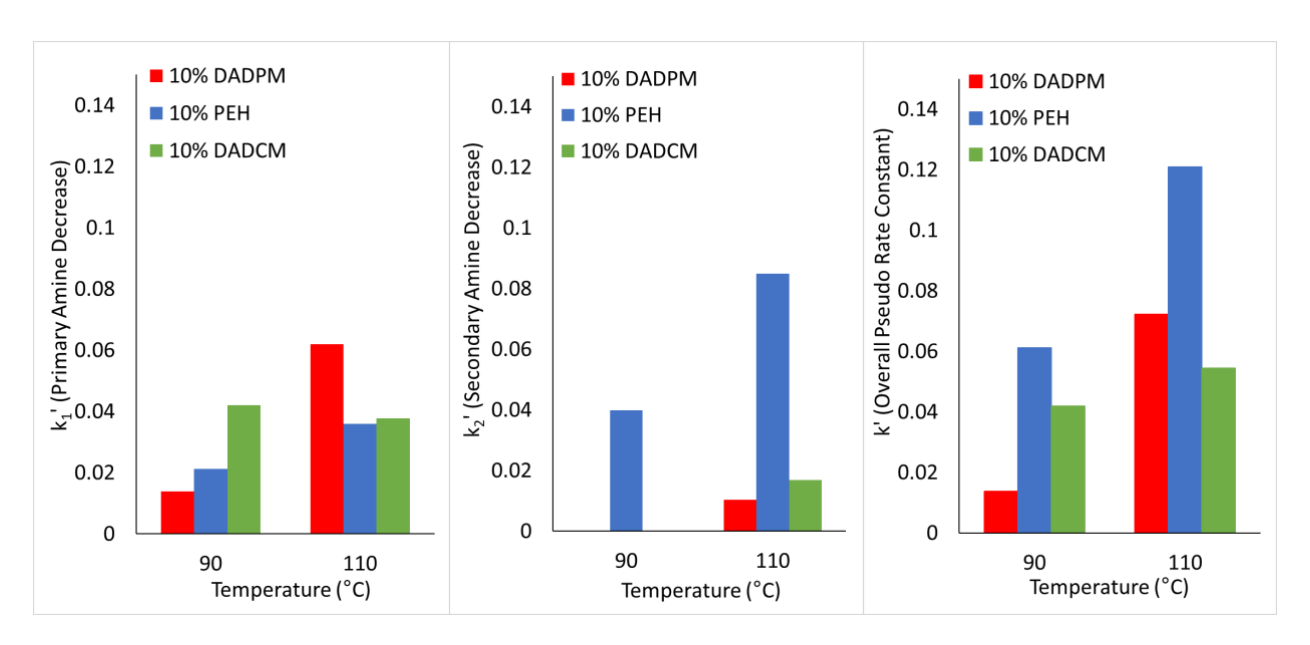


Fig. 14. a. Primary amine (k₁'), b. Secondary amine (k₂'), and c. Cumulative (k') pseudo depletion rate constants for each crosslinker species at set anneal temperatures

These results also indicate that the inherent reactivity of the amine with the Ox-PB is not the dominant factor that controls the strength of the crosslinked interlayer interface. From amine chemistry, one would expect that the aliphatic amines would react more readily than their aromatic counter-parts, but it appears that the aromaticity of the amine conveys significant mechanical strength to the crosslinked interfaces. This observation is consistent with the use of these multi-amines as epoxy curing agents, where they react with epoxides to generate intermolecular crosslinks in a thermoset. Review of the epoxy literature documents how amine curing agents enhance the mechanical, thermal, and chemical resistance of epoxy thermosets, where aromatic structures provide thermosets with increased strength but require higher curing temperatures.^{27, 28} The need for higher reaction temperatures is consistent with the qualitative kinetics in Figure 14, where DADPM reacts more readily at 110 °C. In an epoxy thermoset, cycloaliphatic amines also generate thermal resistance and strength with lower toxicity than aromatic compounds.²⁹ Although the physical improvements are less than with aromatic amines, cycloaliphatic amines are amongst the most used curing agents as they compromise higher reactivity than aromatics and more robust mechanical properties than aliphatic amines. This compromise is mirrored in the results of Figure 14a, where DADCM maintains primary amine reactivity under both annealing conditions while generating consistent interfacial strengthening even when the available heat for the reaction is reduced with print pausing (Fig. 7b). Thus, the results above are consistent with the incorporation of aromatic and cycloaliphatic amines into epoxy resins suitable for more robust applications where mechanical strength is important, as the DADPM and DADCM form the most robust interfaces, particularly at lower amine loadings.

These results therefore indicate that the use of cycloaliphatic or aromatic crosslinking molecules at the interfilament interface provides optimal interfacial strengthening and reactivity that can mitigate structural anisotropy in 3D printed structures. The placement of the crosslinking molecules can be implemented immediately before the deposition of a filament, providing a pathway to utilize available thermal energy of the melted bead for the interfilament reaction. Moreover, this protocol is scalable and readily implemented in most extrusion-based geometries, providing a novel addition to the polymeric 3D printing toolbox that will benefit the growth of 3D printing towards real world manufacturing technologies.

4. Conclusion

These results document a protocol to form covalent bonds between layers in fused filament fabrication printing. Multi-amines deposited between layers in an ABS cube fabricated by FFF during deposition exhibit interlayer interfaces with substantially improved interlayer fracture energy. This strengthening of the interlayer interfaces is

attributed to the reaction of the amines with oxygenated functional groups that form by the oxidation of the ABS filament interface during the printing process. The extent of strengthening of the interface is correlated to the relative reactivity of various multi-amines with oxidized polybutadiene as determined by IR spectroscopy. This correlation indicates that the crosslinking reactions dominate at elevated temperature and thus occur quickly after a filament is deposited. Additional insight indicates that the reactivity of the amine is not the principal factor controlling the strengthening of the interface, rather the aromaticity or cyclic structure of the crosslinker appears to be an important factor in creating robust interfaces. Higher loadings of crosslinker also improve interlayer fracture energy. These results therefore provide an underpinning for expanding this protocol to a broad range of materials and processes in extrusion based additive manufacturing.

Acknowledgement:

MDD acknowledges the support of the U.S. Department of Energy, Office of Science, Basic Energy Sciences, Materials Sciences and Engineering Division. SCP was supported by the National Science Foundation (DMR-1409034 and DMR-1808946).

References

- 1. Kishore, V.; Ajinjeru, C.; Nycz, A.; Post, B.; Lindahl, J.; Kunc, V.; Duty, C., Infrared preheating to improve interlayer strength of big area additive manufacturing (BAAM) components. *Additive Manufacturing* **2017**, *14*, 7-12.
- 2. Duty, C.; Kunc, V.; Compton, B.; Post, B.; Erdman, D.; Smith, R.; Lind, R.; Lloyd, P.; Love, L., Structure and mechanical behavior of Big Area Additive Manufacturing (BAAM) materials. *Rapid Prototyping Journal* **2017**, *23* (1), 181-189.
- 3. Talagani, F.; DorMohammadi, S.; Dutton, R.; Godines, C.; Baid, H.; Abdi, F.; Kunc, V.; Compton, B.; Simunovic, S.; Duty, C.; Love, L.; Post, B.; Blue, C., Numerical Simulation of Big Area Additive Manufacturing (3D Printing) of a Full Size Car. *Sampe Journal* **2015**, *51*, 27.
- 4. Ahn, S.-H.; Montero, M.; Odell, D.; Roundy, S.; Wright, P. K., Anisotropic material properties of fused deposition modeling ABS. *Rapid Prototyping* **2002**, *8* (4), 248-257.
- 5. Bellini, A.; Guceri, S., Mechanical characterization of parts fabricated using fused deposition modeling. *Rapid Prototyping* **2003**, *9* (4), 252-264.
- 6. Es-Said, O. S.; Foyos, J.; Noorani, R.; Mendelson, M.; Marloth, R.; Pregger, B. A., Effect of Layer Orientation on Mechanical Properties of Rapid Prototyped Samples. *Materials and Manufacturing Processes* **2000**, *15* (1), 107-122.
- 7. Levenhagen, N. P.; Dadmun, M. D., Bimodal molecular weight samples improve the isotropy of 3D printed polymeric samples. *Polymer* **2017**, *122*, 232-241.
- 8. Bellehumeur, C.; Li, L.; Sun, Q.; Gu, P., Modeling of Bond Formation Between Polymer Filaments in the Fused Deposition Modeling Process. *Journal of Manufacturing Processes* **2004**, *6* (2), 170-178.
- 9. Agrawal, G.; Wool, R. P.; Dozier, W. D.; Felcher, G. P.; Zhou, J.; Pispas, S.; Mays, J. W.; Russell, T. P., Interdiffusion of polymers across interfaces. *Journal of Polymer Science Part B: Polymer Physics* **1996**, *34* (17), 2919-2940.
- 10. Wool, R. P.; Willett, J. L.; McGarel, O. J.; Yuan, B. L., Strength of polymer interfaces. *Am. Chem. Soc. Polym. Prepr. Div. Polym. Chem.* **1987**, *28* (2), 38-39.
- 11. Hossain, M. S.; Ramos, J.; Espalin, D.; Perez, M.; Wicker, R., Improving tensile properties of FDM manufactured specimens via modifying build parameters. *Journal of Manufacturing Science and Engineering* **2014**, *136* (6), 380-392.
- 12. Huang, B.; Singamneni, S., Raster Angle Mechanics in Fused Deposition Modeling. *Journal of Composite Materials* **2014**, *49* (3), 363-383.
- 13. Davidson, J. R.; Appuhamillage, G. A.; Thompson, C. M.; Voit, W.; Smaldone, R. A., Design Paradigm Utilizing Reversible Diels–Alder Reactions to Enhance the Mechanical Properties of 3D Printed Materials. *Applied Materials and Interfaces* **2016**, *8*, 16961-16966.
- 14. Waheed, S.; Cabot, J. M.; Smejkal, P.; Farajikhah, S.; Sayyar, S.; Innis, P. C.; Beirne, S.; Barnsley, G.; Lewis, T. W.; Breadmore, M. C.; Paull, B., Three-Dimensional Printing of Abrasive, Hard, and Thermally Conductive Synthetic Microdiamond–Polymer Composite Using Low-Cost Fused Deposition Modeling Printer. *ACS Appl. Mater. Interfaces* **2019**, *11*, 4353-4363.
- 15. Rostom, S.; Dadmun, M. D., Improving heat transfer in fused deposition modeling with graphene enhances inter filament bonding. *Polymer Chemistry* **2019**, *10*, 5967-5978.
- 16. Guyader, M.; Audouin, L.; Colin, X.; Verdu, J.; Chevalier, S., Epoxides in the theral oxidation of polybutadiene. *Polymer Degradation and Stability* **2006**, *91*, 2813-2815.
- 17. Duh, Y.-S.; Ho, T.-C.; Chenn, J.-R.; Kao, C.-S., Study on Exothermic Oxidation of Acrylonitrile-butadienestyrene (ABS) Resin Powder with Application to ABS Processing Safety. *Polymer* **2010**, (2), 174-187.
- 18. Adeniyi, J. B.; Kolawole, E. G., Thermal and Photo-Degradation of Unstabilized ABS. *European Polymer Journal* **1984**, *20* (1), 43-47.

- 19. Martin, R. B., Reactions of Carbonyl Compounds with Amines and Derivatives. *Journal of Physical Chemistry* **1963**, *68* (6), 1369-1377.
- 20. Aliheidari, N.; Tripuraneni, R.; Ameli, A.; Nadimpalli, S., Fracture resistance measurement of fused deposition modeling 3D printed polymers. *Polymer Testing* **2017**, *60*, 94-101.
- 21. William A. Henderson, J.; Schultz, C. J., The Nucleophilicity of Amines. *J. Org. Chem.* **1962,** *27* (12), 4643-4646.
- 22. Lee, H.; Neville, K., Handbook of Epoxy Resins. 1967.
- 23. Chapman, N. B.; Isaacs, N. S.; Parker, R. E., 386. The mechanism of epoxide reactions. Part I. The reactions of 1: 2-epoxyethylbenzene, 1: 2-epoxy-3-phenylpropane, and 1: 2-epoxy-3-phenoxypropane with some secondary amines. *Journal of the Chemical Society (Resumed)* **1959**, (0), 1925-1934.
- 24. Badawi, H. M., A comparative study of the structure and vibrational spectra of diphenylmethane, the carcinogen 4,4'-methylenedianiline and 4,4'-methylenebis(N,N-dimethylaniline). *Spectrochimica Acta Part A: Molecular and Biomolecular Spectroscopy* **2013**, *109*, 213-220.
- 25. Horie, K.; Hiura, H.; Sawada, M.; Mita, I.; Kambe, H., Calorimetric investigation of polymerization reactions. III. Curing reaction of epoxides with amines. *Journal of Polymer Science Part A-1: Polymer Chemistry* **1970**, *8* (6), 1357-1372.
- 26. Rondan, N. G.; Marks, M. J.; Hoyles, S.; Pham, H., paper presented at the *225th ACS National Meeting*. **2003**.
- 27. Fedtke, M.; Domaratius, F.; Pfitzmann, A., Curing of epoxy resins with dicyandiamide. *Polymer Bulletin* **1990**, *23* (4), 381-388.
- 28. Ellis, B., *Chemistry and Technology of Epoxy resins*, 1st ed. . Ashcroft, W. R., Ed. Blackie Academic and Professional Glasgow, U.K., 1993; pp 37, 71.
- 29. Pham, H. Q.; Marks, M. J., Epoxy Resins. *Ullmann's Encyclopedia of Industrial Chemistry* **2005**.